Simulation of cortico-basal ganglia oscillations and their suppression by closed loop deep brain stimulation

Peadar F. Grant*, *Member, IEEE* and Madeleine M. Lowery, *Member, IEEE*

University College Dublin

in: IEEE Transactions on Neural Systems and Rehabilitation Engineering. See also BIBTEX entry below.

document created on: September 12, 2012
created from file: nmpaper.tex
cover page automatically created with CoverPage.sty
(available at your favourite CTAN mirror)

Simulation of cortico-basal ganglia oscillations and their suppression by closed loop deep brain stimulation

Peadar F. Grant*, *Member, IEEE* and Madeleine M. Lowery, *Member, IEEE*

***Abstract*—A new model of deep brain stimulation is presented that integrates volume conduction effects with a neural model of pathological beta-band oscillations in the cortico-basal ganglia network. The model is used to test the clinical hypothesis that closed-loop control of the amplitude of DBS may be possible, based on the average rectified value of beta-band oscillations in the local field potential. Simulation of closed-loop high-frequency Deep Brain Stimulation was shown to yield energy savings, with the magnitude of the energy saved dependent on the strength of coupling between the subthalamic nucleus and the remainder of the cortico-basal ganglia network. When closed-loop DBS was applied to a strongly coupled cortico-basal ganglia network, the stimulation energy delivered over a 480 s period was reduced by up to 42 %. Greater energy reductions were observed for weakly coupled networks, as the stimulation amplitude reduced to zero once the initial desynchronization had occurred. The results provide support for the application of closed-loop high-frequency DBS based on electrophysiological biomarkers.**

***Index Terms*—closed-loop deep brain stimulation, computational model**

I. Introduction

DEEP Brain Stimulation (DBS) is a modern clinical therapy in which surgically implanted electrodes are used to deliver continuous stimulation in the treatment of movement and psychiatric disorders. Having achieved widespread acceptance in the control of the main motor symptoms of Parkinson's Disease, DBS is now being considered as a treatment for many other conditions. Despite its success in the treatment of Parkinson's Disease, fundamental questions about the mechanisms by which DBS achieves its effects remain unanswered. As a consequence, it is not entirely clear how the delivered therapy may be optimised on an ongoing basis.

DBS as currently applied in open-loop configuration can not adapt to changes in symptom severity or other factors such as variations in the electrode-tissue interface or encapsulation tissue. Stimulus parameters may not necessarily be optimised at any given time for a given task. In addition, the constant application of DBS at a fixed amplitude may consume more power than necessary, which may require compromises to be made when choosing stimulus parameters [1]. As a result, there has been considerable interest amongst researchers, clinicians and device manufacturers in developing methods of closed-loop DBS. Closed-loop stimulation offers the possibility to continuously optimise the delivered stimulus to the symptom severity whilst avoiding undesirable side-effects, and may reduce the power consumption of stimulation devices by reducing the stimulus intensity when possible.

Electrophysiological investigations have linked the power of oscillations in the tremor (4 Hz to 8 Hz) and beta-band (11 Hz to 30 Hz) frequency ranges of local field potential (LFP) data recorded from DBS electrodes to both tremor and akinetic symptoms [2], [3], [4], [5], [6], [7]. LFP recordings have additionally shown that the application of DBS or Levodopa attenuates beta-band synchronised oscillations in the course of suppressing symptoms [8], [9]. Based on these observations, it has been suggested that it may be possible to apply closed-loop DBS based on the strength of oscillatory activity within specific frequency bands in the LFP [8], [9].

Two main paradigms for delivering closed-loop DBS have been proposed. The first uses high-frequency DBS waveforms as currently used in open-loop configuration, but applies closed-loop control to vary the stimulation parameters [10]. The second, termed "mild stimulation", attempts to desynchronise pathological oscillatory networks in an on-demand fashion [11], [12], [13], [14]. At present, the only implanted stimulation hardware for closed-loop DBS that has been proposed for clinical use is designed to deliver high-frequency DBS [15]. Previous computational models have been developed that aim to improve the efficacy of DBS through closed-loop control of the DBS amplitude [10], and to reduce the energy delivered during stimulation by the automated design of novel stimulation waveforms [16], [17]. Closed-loop control of the DBS amplitude has been shown to be capable of restoring the LFP power spectrum of a parkinsonian STN population to approximate physiological conditions, but the model did not incorporate cortico-basal ganglia feedback [10]. In addition, side effects of DBS due to activation of adjacent fibers [18], could potentially be reduced by a lowered average stimulation amplitude.

Computational modelling offers a means to further develop and test the feasibility of closed-loop high-frequency stimulation paradigms by investigating and tuning control schemes based on biomarkers of symptom severity. An ideal model would capture the DBS waveform generated, the resulting electric field distribution and neural activation patterns, closed-loop network activity and neuromodulation effects. In addition, the model should provide an estimate of the LFP to enable the level of oscillatory activity to be quantified and to provide

P.F. Grant is with the UCD School of Electrical, Electronic and Communications Engineering, University College Dublin, Dublin, Ireland. (e-mail: peadargrant@gmail.com)

M.M. Lowery is with the UCD School of Electrical, Electronic and Communications Engineering, University College Dublin, Dublin, Ireland.

a feedback signal for controlling the applied stimulation. Computational models of DBS at present do not capture all of these features and have tended to focus either on volume conduction or network effects in isolation from one another.

Physiologically-based network models capture the activity of each nucleus (STN, GPe, GPi, cortex, thalamus etc.) using a large number of model neurons [19]. The primary limitations of networks based around a large number of physiological or simplified discrete neural oscillators is the high computational burden of solution due to the complexity involved in their interconnection to volume conductor models. As a result, volume conductor models that calculate the electric field due to the applied stimulation, and thereby estimate the volume of tissue activated in complex inhomogeneous geometries, have not yet been combined with models of the thalamo-cortico-basal ganglia network.

In contrast to the high complexity of physiologically-based networks, low-dimensional phenomenological models that simulate the synchronised mean-field oscillations of interconnected nuclei have also been proposed. Since they are based on standard linear and nonlinear components, for example sigmoidal nonlinearities and linear filters, existing optimisation and control-theory tools may be applied to understand their behaviour [20]. However, such models lack a physical interface through which to record local field potentials and apply DBS, since the model parameters are representative of the mean field oscillations arising from the synchronised activity of large numbers of neurons rather than physiologically measurable signals, such as individual membrane voltage or ionic currents.

As in the case of physiologically-based network models, there remains a disconnect between phenomenological models and volume conductor models of DBS. There may be an opportunity, however, to augment phenomenological mean-field models with aspects of more physiological neuron models to enable certain populations of neurons to be represented in a more realistic fashion. This combination could allow volume conductor effects to be incorporated in a network while retaining the computational efficiency and analytical advantages of simplified models. To date, this approach has not yet been explored.

The aim of this study was to investigate the use of closed-loop integral control to modulate DBS amplitude by constructing a novel network model of the nuclei involved in the generation of pathological beta-band oscillations, coupled to a volume conductor model. The proposed model combined components of a physiological neural network with concepts from phenomenological mean-field modelling, in order to address the disconnect that exists between models that examine the volume of tissue influenced by the electric field and the resulting effects on pathological oscillations in the closed-loop cortico-basal ganglia networks. The predicted energy requirement to suppress beta band oscillations under closed-loop stimulation was compared to that required under open-loop stimulation to quantify the potential benefits of moving from open-loop parameter setting to closed-loop control in terms of power consumption. The performance of the closed-loop stimulation was investigated as the strength of coupling within the cortico-basal ganglia network was altered during the stimulation period to promote the growth of additional beta-band oscillations to illustrate the ability of the closed-loop control system to respond to changes in the network activity.

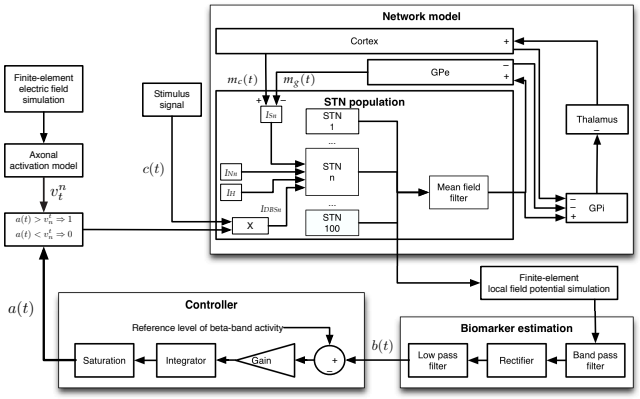

Fig. 1. Schematic diagram of model, showing DBS signal and resulting electric field model used to estimate axonal activation, which controls the current I_{DBS} of each single-compartment STN cell in the STN neuron model. Each STN cell also receives individually calculated synaptic, I_S^n and noise, I_N^n, currents. All STN cells receive 1 nA hyperpolarizing current I_H. The STN is part of the network model that incorporates the Cortex, GPe, Thalamus and GPi as neural mass elements. The local field potential recorded from the STN is simulated, and its average rectified value is passed into the integral controller, which modulates the amplitude of the DBS signal. The volume conductor model (not shown) is used to simulate the electric field and local field potential.

II. Methods

To investigate the neuromodulative effects of the electric field produced by DBS, a new model was developed in which a model of volume conduction in the tissue surrounding the DBS electrode was integrated with a network model of pathological beta-band oscillations within the cortico-basal ganglia network. The network model simulated the generation of beta-band parkinsonian oscillations in the basal ganglia, incorporating physiologically-based STN neurons together with simplified lumped representations of the cortex, thalamus, GPi and GPe. The electric field and resulting activation of STN axons due to applied DBS was estimated for a given stimulation voltage, using a volume conductor model in conjunction with an STN axon model. It was assumed that DBS achieves its therapeutic effect through axonal activation [21], [22], and that the application of DBS suppressed STN activity entirely. The LFP recorded at the DBS electrode was also simulated, and the average rectified value (ARV) of the LFP was used as a biomarker of the level of beta-band activity. Closed-loop control of the DBS stimulation amplitude was then applied to reduce the amplitude of the beta-band oscillatory activity. A schematic diagram of the model is presented in Figure 1.

A. Volume-conductor model

A volume conductor model was implemented to estimate the electric field resulting from DBS and to simulate the local field potential. The conducting volume of an adult human head was represented by an idealised ellipsoidal finite-element model, based on the model developed in [23]. The whole-head model

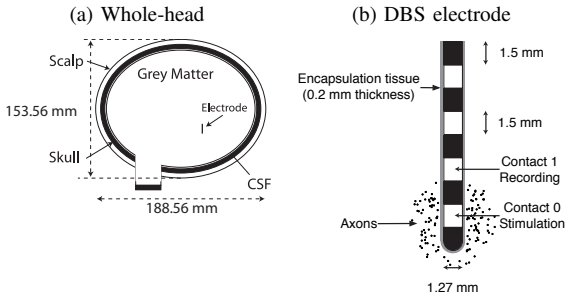

Fig. 2. Schematic of (a) volume conductor model and (b) DBS electrode with surrounding axon distribution. Schematics are to different scales.

TABLE I
TISSUE CONDUCTIVITIES, σ, AND THICKNESSES, d_m, USED IN THE VOLUME CONDUCTOR MODEL. CONDUCTIVITIES WERE CALCULATED AT 2560 Hz FOR A PULSE WIDTH OF 100 µs AND A PULSE FREQUENCY OF 130 Hz. SOURCES: [A] SCHEUFLER *et al.* [29], [B] INTERNATIONAL COMMISSION ON RADIOLOGICAL PROTECTION [30], [C] BUTSON *et al.* [31], [D] GABRIEL *et al.* [32], [E] BAUMANN *et al.* [33], [F] RANCK AND BEMENT [34], [G] GRILL AND MORTIMER [27].

Layer	d_m **(mm)**	σ **(S m^{-1})**
Scalp	3.1 [A]	0.042 [D]
Skull	0.8 [B]	0.020 [D]
CSF	1.8 [B]	1.60 [E]
Brain tissue	—	0.27 [F]
Encapsulation tissue	0.2 [C]	0.042 [G]

allowed the finite nature of the head and electrical grounding effects of the stimulation system to be incorporated [23], [24]. A Medtronic 3387 electrode [25], radius 0.635 mm and contact height 1.5 mm, was simulated to lie within in the model, as described in at the location of the subthalamic nucleus [26]. A cylindrical encapsulation layer surrounding the DBS electrode was included to incorporate resistive effects resulting from the formation of collagen, fibroblasts and giant cells, which reduce the voltage developed in the tissue for a given stimulus [27]. The encapsulation region was assumed to be 200 µm thick. The boundary surface where the spinal cord enters the skull was designated as the electrical reference ground. To reduce the computational complexity of the model, the entire scalp region was assumed to consist of non-infiltrated fat tissue and the entire skull region was assumed to consist of cortical bone, as in [28]. Schematics of the whole-head geometry and DBS electrode are presented in Figure 2. The material properties used were identical to those in [23], and are summarised together with the model dimensions in Table I.

The geometry was discretised into 95,280 linear tetrahedral elements. The Laplace equation was solved to calculate the electric potential distributions resulting from the applied voltage controlled stimulus

$$-\nabla \cdot \sigma \nabla \phi = 0 \tag{1}$$

where σ is the electrical conductivity and ϕ, the independent variable, is the electric potential. DBS was applied to the surface of the most distal electrode contact on the Medtronic 3387 DBS implant, numbered Contact 0 in [25].

The distribution of the electric potential estimated using the volume conductor model was used to calculate the threshold voltage necessary to activate the STN axons described in Section II-B. The volume conductor was also used to simulate the LFP recorded by the DBS electrode as described in Section II-F.

B. Threshold voltage for activation of STN neurons

To estimate the axonal activation due to the electric potential distribution resulting from DBS, the threshold stimulus voltage was calculated for 100 parallel axons randomly distributed within a radius of 0.835 mm to 3 mm from the centre of the DBS electrode, where the electrode was assumed to be centred within the STN [18], Figure 2(b). The axon model was based on that developed in [35]. Each axon consisted of 20 compartments with 500 µm inter-nodal spacing, giving an axon length of 10 mm. The threshold of activation of each axon, defined as the voltage at which the axon fires in synchrony with the DBS stimulus, was determined for a pulse of duration of 60 µs at a frequency of 130 Hz, where the charge-balance pulse was 0.2 times the amplitude and 5 times the duration of the stimulation pulse. A lookup table was constructed, which contained the threshold voltage of axonal activation for a given axon n, v_t^n. The threshold voltages were used to determine which STN neurons were activated by a particular DBS waveform in the network model, Figure 1. The axon model was used only to determine whether a particular STN neuron was activated by DBS, and was not utilised further in the network model.

C. Network model

A network model was constructed to simulate the increased beta-band oscillations that arise in the cortico-basal ganglia system, in order to investigate their suppression by DBS. Increased synchronised oscillatory activity within the cortico-basal ganglia is associated with Parkinson's Disease [36]. The increased synchronisation has been attributed to changes in synaptic coupling, where certain pathways in the cortico-basal ganglia network become strengthened and others weakened [37], [38]. In particular, the sensitivity of STN neurons to excitatory inputs from the cortex has been shown to increase under conditions of dopamine depletion [39], [40].

It has also been shown that the mean field of a large number of neurons when firing in a synchronised fashion may be represented by an almost-sinusoidal oscillation [12], [41]. This type of oscillation may be simulated using phenomenological mean-field models, where the dynamics are incorporated in linear filter elements, and synaptic coupling strength or excitably is incorporated in static nonlinearities [20].

Tremor band oscillations due to the interaction between the STN and the GPe and their suppression by DBS were simulated using linear filters in cascade with sigmoidal nonlinearities in a previous study [20]. A similar approach was used in this study, where synchronised beta-band activity was modelled by simulating an oscillatory hyperdirect loop [37] formed by STN, GPi, thalamus and cortex. Increased strength of the cumulative synaptic coupling within the loop due to strengthening of the hyperdirect pathway from the cortex to

TABLE II
NONLINEAR GAIN VALUES AND LOW-PASS FILTER COEFFICIENTS OF LUMPED NUCLEI INCORPORATED IN MODEL.

Nucleus	Slope	Numerator	Denominator		
	s	p_0	q_2	q_1	q_0
Cortex	1.1	16000	1×10^{12}	30×10^6	16000
GPe	1.1	16000	1×10^{12}	10×10^6	16000
Thalamus	1.1	16000	1×10^{12}	40×10^6	16000
GPi	1.1	2902	1×10^{12}	40×10^6	1200

the STN, associated with dopamine depletion, was modelled by increasing the cortico-basal ganglia loop gain to promote the onset of beta-band oscillations [37]. The inhibitory effect of the cortex on the GPi through the activation of the striatum was also simulated by inhibition of the GPi [42].

The GPi, cortex, thalamus and GPe were each implemented using a sigmoidal nonlinearity in cascade with a second order linear low-pass filter. The sigmoidal nonlinearities have the characteristic:

$$v_o = \arctan \frac{v_i}{s} \tag{2}$$

where $\frac{1}{s}$ is the slope at the origin, which may be taken as a measure of the "gain" of the nonlinearity and v_i is the input signal to the nonlinearity. Increased strength of the synaptic coupling is simulated by reducing s, thereby increasing the gain around the loop. The second-order filters have the following transfer function:

$$H(j\omega) = \frac{p_0}{q_2(j\omega)^2 + q_1(j\omega) + q_0} \tag{3}$$

The Barkhausen criterion for oscillation requires the loop gain equal to unity with no phase shift for oscillation to be sustained at a given frequency. To establish oscillations, simulating conditions of dopamine depletion, the gain around the loop was increased by increasing s^{-1} at each of the sigmoidal nonlinearities in the GPi, thalamus, cortex and GPe until the loop gain exceeded unity, Equation 2. The amplitude of oscillation is limited by the characteristic of the sigmoidal nonlinearity, thereby achieving an almost-sinusoidal oscillation. Filter coefficients were altered from those given in [20] to achieve oscillations in the beta-band frequency range. The parameters for the blocks representing the GPe, GPi, thalamus and cortex are given in Table II. The network structure is shown in Figure 1.

To allow the effects of the electric field due to DBS on the STN to be incorporated, the lumped model of the STN used in [20] was replaced with a model comprised of 100 individual STN neurons, each associated with an axon located within the volume conductor model

D. STN neuron model

In the network model, the dynamical input-output behaviour of each STN neuron was subsumed into a single-compartment model, based on that developed by [43]. This STN model captures the mechanisms underlying the plateau potentials that are believed to play a critical role in the generation of parkinsonian bursting neural activity [44]. The behaviour of the single-compartment STN neuron n, which subsumed the behaviour of the soma and axon in the network model, was described by the equation:

$$\begin{aligned} C_m^n \tfrac{\mathrm{d}V_m^n}{\mathrm{d}t} = &- I_{Na}^n - I_K^n - I_A^n - I_L^n - I_T^n - I_{Ca-K}^n - I_l^n \\ &- I_H - I_N^n + I_S^n + I_{DBS}^n \end{aligned} \tag{4}$$

The ionic current channels included are the sodium, I_{Na}^n, high activation threshold potassium I_K^n, low activation threshold potassium I_A^n, long-lasting calcium currents I_L^n, low-threshold calcium currents I_T^n, calcium-activated potassium I_{Ca-K}^n and leakage I_l^n currents. Membrane capacitance, C_m^n, in addition to channel activation and inactivation parameters were set equal to those reported in Table 1 of [43].

Additional current inputs were included to model hyperpolarising currents, synaptic noise and synaptic coupling from the cortex and GPe to the STN. A hyperpolarising current I_H of 1 nA was applied to each neuron to promote the generation of burst firing and accompanying plateau potentials, shown to be associated with dopamine depletion under parkinsonian conditions in rats [43]. Low-amplitude, uniformly distributed band-limited white noise, I_N^n, was added to the transmembrane current of each neuron to simulate synaptic noise.

The synaptic current inputs were represented by I_S^n. Since the model consists of multiple pathways it was necessary to include contributions from the mean fields of the GPe and cortical blocks, $m_g(t)$ and $m_c(t)$ respectively, projecting on to the individual STN neurons. In the model, each STN neuron could be synaptically connected to the GPe, cortex, both or none. The connectivity is described in the following section, Section II-E

The effect of DBS on the STN model was implemented through the current I_{DBS}^n as presented in Figure 1. Each STN neuron, n, fired in synchrony with the 130 Hz DBS signal when the DBS amplitude, $a(t)$, exceeded the threshold voltage for axonal activation of neuron n, v_t^n. To implement this, a stimulus signal, $c(t)$, of sufficient amplitude to fire the single-compartment STN model, was added to the transmembrane current when the threshold voltage for axonal activation of neuron n was exceeded.

$$I_{DBS}^n(t) = \begin{cases} c(t) & \forall \quad a \geq v_t^n \\ 0 & \forall \quad a < v_t^n \end{cases} \tag{5}$$

E. Connectivity

In this study, two STN populations with different strengths of synaptic coupling were studied. In both cases, a neuron could be coupled to one, both or neither of the GPe and cortex, according to the interconnection matrix in Equation 6. For each neuron n, the parameter $x_c^n = 1$ if the neuron receives the mean field input from the cortex, otherwise x_c^n is zero. The parameter x_g^n similarly sets whether the neuron n receives input from the GPe. The signals $m_g(t)$ and $m_c(t)$ denote the mean field from the GPi and cortex respectively.

$$\begin{pmatrix} I_S^1 \\ I_S^2 \\ \dots \\ I_S^{100} \end{pmatrix} = \begin{pmatrix} x_g^1 & x_c^1 \\ x_g^2 & x_c^2 \\ \dots & \dots \\ x_g^{100} & x_c^{100} \end{pmatrix} \begin{pmatrix} m_g(t) \\ m_c(t) \end{pmatrix} \tag{6}$$

Under conditions of *strong coupling*, 50 % of the STN neurons selected at random received cortical input, whilst another 50 % selected at random received inputs from the GPe. Under conditions of *weak coupling*, 25 % of STN neurons received input from the GPe, whilst 25 % of the STN population received cortical input. The mean-field signal from the full STN population was input to the lumped GPi and GPe components of the network model, Figure 1.

F. Simulation of the local field potential

The volume conductor described in Section II-A was used to numerically simulate the LFP resulting from postsynaptic potentials incident on the STN neurons from GPe and cortical inputs by solving the Laplace equation, Equation 1. In this model, the point current source contribution from each STN neuron to the LFP signal was equal to the sum of the mean-field signals from the cortex and GPe projecting to that neuron. The theorem of reciprocity was applied to simulate the LFP signals, allowing the voltage at a recording electrode due to a number of point current sources to be calculated as the sum of the potentials at each source location due to a single point current source located at the recording electrode. The LFP recording also included the stimulation artefact due to the applied DBS signal on the electrode contact used for stimulation, Contact 0. Monopolar LFP recordings from the second most distal contact, Contact 1, on the Medtronic 3387 electrode lead were simulated in this way, while the DBS signal was applied at the most distal contact, Contact 0 [25]. The LFP signal recorded at Contact 1, $l(t)$, was calculated as the integral of the electric potential ϕ evaluated over the entire surface area S of Contact 1 divided by the surface area S, where $\mathrm{d}S$ denotes an elemental surface area.

$$l(t) = \frac{1}{S}\left(\int_S \phi(t)\,\mathrm{d}S\right) \tag{7}$$

G. Biomarker estimation

To investigate the hypothesis that beta-band oscillatory activity may be a suitable biomarker for closed-loop control of DBS [8], [5], [9], the ARV of the beta-band oscillations in the STN, was calculated. The LFP recorded from the DBS electrode, $l(t)$, was band-pass filtered from 12 Hz to 30 Hz using a Chebyshev Type 1 filter, full wave rectified and averaged by low-pass filtering at 2 Hz. Since the lowest component of the idealised DBS waveform used was at 130 Hz, substantially greater than the upper stop-band of the frequency selection filter, no further artefact removal was necessary in this simulation study, Figure 3. The governing equation for the ARV of the LFP, $b(t)$, where h_b and h_l describe the impulse responses of the band-pass and low-pass filters respectively is

$$b(t) = h_l(t) * \left|l(t) * h_b(t)\right| \tag{8}$$

The signal $b(t)$ yielded a biomarker reflecting the magnitude of beta-band oscillations with which to examine closed-loop control.

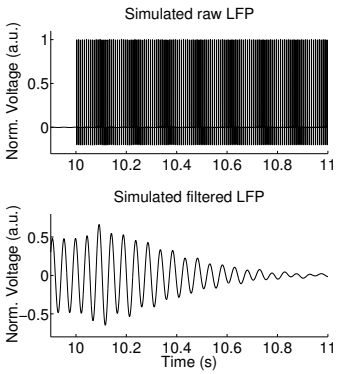

Fig. 3. (Top) Simulated raw local field potential includes artifact due to stimulation. (Bottom) Filtered local field potential, which does not include stimulus artifact as it is outside the passband of the band-pass filter in the biomarker estimation circuit.

H. Controller

The ARV of the simulated LFP was used to modulate the amplitude of DBS. The reference signal for the controller was the target level of beta-band oscillatory activity, which in practice would be chosen based on a patient-specific basis to achieve an appropriate balance between symptom suppression and power conservation. In this study the target value of the ARV of the LFP, b_r, during stimulation was set to 5 % of the magnitude of the biomarker signal prior to DBS application. This arbitrary choice represents an almost complete suppression of beta-band activity, although in clinical practice it may be desired to allow a healthy level of beta-band activity to remain [9]. The error signal was calculated as the difference between the reference signal and the ARV of the LFP. The maximum allowed stimulation voltage was limited to that required to stimulate all neurons within the STN. Integral control of the DBS amplitude was chosen as it does not introduce a steady-state error, as would be the case with proportional control [45]. It is envisaged that in practice the controller gain, k, biomarker reference level, b_r, and the maximum stimulus amplitude, a_m, would be chosen clinically on a patient-specific basis. The controller, presented in Figure 1, modulates the amplitude $a(t)$ of the DBS waveform, according to the governing equation:

$$a(t) = k\int (b(t) - b_r)\,\mathrm{d}t \tag{9}$$

where $a(t)$ cannot exceed the maximum stimulus amplitude a_m. It was further assumed that $a(t)$ varied slowly and remained constant during one cycle of the DBS waveform. An integrator gain k of 1 was chosen initially. In addition, integrator gains of 2, 5 and 10 were investigated when comparing the performance of closed-loop to open-loop stimulation.

I. Simulation details

The electric field distribution due to DBS was calculated using COMSOL 3.5a (COMSOL AB, Stockholm, Sweden). The STN axons were simulated using the NEURON simulation environment [46]. All other network components, including the STN neurons, were implemented using Simulink

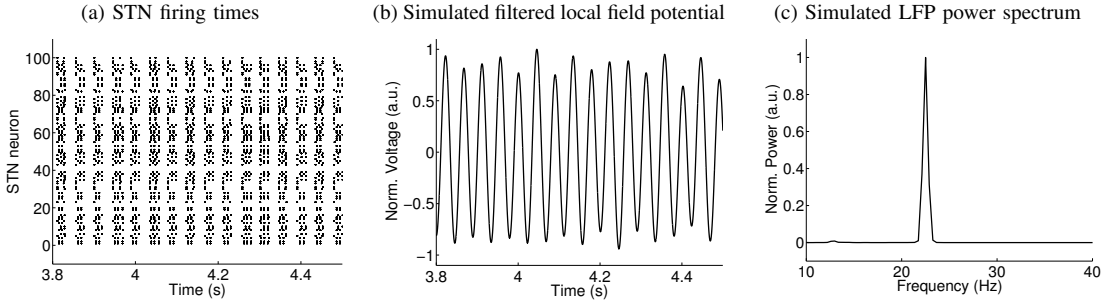

Fig. 4. (a) STN firing times, (b) simulated filtered local field potential, (c) power spectrum of local field potential.

(Mathworks, Natick, MA). The time step used in network simulations was 0.01 ms, and 500 s of data was simulated, using fixed-step first order numerical integration. Simulations were allowed to run for 5 s before storing the output data to allow startup transients to disappear and the oscillations to stabilise. DBS was activated at $t = 10\,\mathrm{s}$ and remained active until $t = 490\,\mathrm{s}$. Each simulation of 500 s of real-time data required approximately 12 hours using a quad-core AMD64-architecture CPU.

To examine response of the controller to changing conditions, temporary increases in the beta-band oscillations were simulated by increasing the slope or nonlinear gain of the $\arctan$ functions of the sigmoidal nonlinearities used to represent the GPi, GPe, cortex and thalamus. This represents a sudden increase in the gain around the entire loop, promoting the establishment of pathological oscillations during the time period $t = 200\,\mathrm{s}$ to $t = 300\,\mathrm{s}$.

III. Results

A. Determination of axonal thresholds

The threshold voltages for activation of the STN axons by the 130 Hz, 60 µs DBS stimulus were distributed between 0.18 V for the axons located closest to the electrode at 0.835 mm from the centre of the active contact and 0.51 V for axons furthest from the electrode, 3 mm from the centre of the active contact. This was used subsequently to control the number of STN cells determined to be synchronised to the stimulus with respect to the stimulus amplitude.

B. Generation of pathological oscillations in the STN

When the parameter controlling the loop gain, s^{-1}, was increased from 0 to 1.1, burst firing of the STN neurons at approximately 22 Hz, which lies within the beta band (11 Hz to 30 Hz), was observed. The firing patterns of individual neurons were observed to exhibit burst firing and plateau potentials similar to results reported experimentally in rats under parkinsonian conditions [43]. The firing patterns of the STN population are presented in Figure 4, along with the simulated LFP. The power spectrum of the resulting local field potential indicated an almost sinusoidal oscillation, with a single peak at 22 Hz.

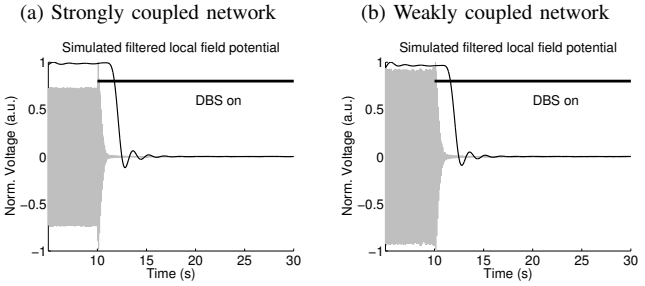

Fig. 5. Suppression of oscillations through the application of open-loop DBS of amplitude 0.51 V, frequency 130 Hz and pulse duration 60 µs. The simulated filtered LFP recorded from the STN is shown in grey and the ARV of the LFP is shown in black, normalized to the maximum amplitude of the simulated LFP.

C. Open-loop DBS

The simulated pathological oscillations, promoted by a loop gain greater than unity, were suppressed by the application of open-loop DBS at an amplitude 0.51 V. The reduction in the beta-band LFP and resulting biomarker when DBS was applied are presented in Figure 5 for each of the two networks considered. The attenuation of the oscillatory activity shown by the model was similar to that observed during electrophysiological studies [6].

D. Closed-loop DBS

Using integral control based on the error between the target beta-band oscillation amplitude and the biomarker of beta-band activity resulted in modulation of the DBS amplitude as shown in Figure 6 for a controller gain $k = 1$. Controller parameters were identical in the strongly and weakly coupled cases. When the STN was strongly coupled to the cortex and the GPe, the DBS amplitude increased to activate all STN neurons in the population to quench the pathological oscillations, Figure 6(a). The amplitude then reduced to maintain the target level of oscillatory activity in the beta-band. When the STN was weakly coupled to the cortex and the GPe, it was observed that the amplitude of the DBS signal could be reduced to zero once desynchronisation had been achieved, Figure 6(b).

To investigate the effect of varying controller gain on the reduction in the stimulus energy, additional simulations were conducted at gain values of 2, 5 and 10. The effect of increasing gain depended on the strength of the STN-network coupling. The reductions in the DBS signal energy resulting

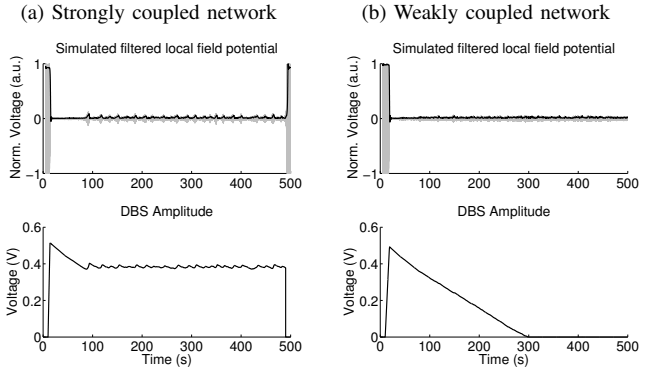

Fig. 6. Suppression of oscillations through the application of closed-loop DBS of pulse duration 60 µs and pulse frequency 130 Hz. The simulated filtered LFP recorded from the STN (grey) and the ARV of the LFP are normalized to the maximum amplitude of the simulated LFP. The controller modulates the applied DBS amplitude. The controller gain k was set to 1. DBS artifact has been removed from the LFP by filtering.

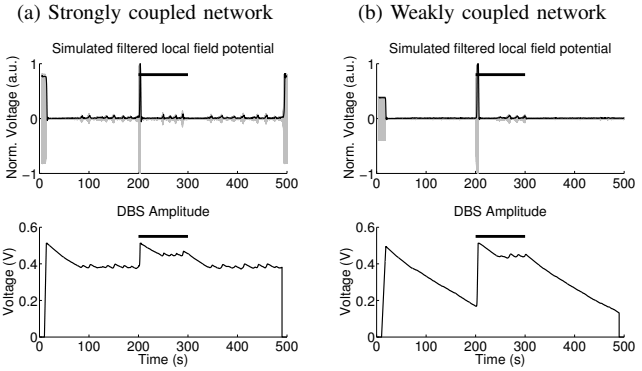

Fig. 7. Adaptation of DBS amplitude to increased beta-band activity. Additional beta-band activity was promoted by increasing the gain of the nonlinearities in the cortex, thalamus, GPe and GPi by reducing the parameter s from 1.1 to 0.8 during the interval 200 s to 300 s, shown by the black bar. The controller modulates the applied DBS amplitude. The controller gain k was set to 1. DBS artifact is not present in the band-pass filtered LFP (grey).

TABLE III
PERCENTAGE REDUCTION IN THE ENERGY OF THE DBS SIGNAL REQUIRED TO REDUCE THE ARV OF THE LFP TO 5 % OF ITS VALUE BEFORE DBS WAS ACTIVATED COMPARED TO OPEN-LOOP DBS.

Network	Controller gain	Energy reduction
Strongly coupled	1	41.6 %
	2	41.9 %
	5	41.4 %
	10	39.1 %
Weakly coupled	1	83.5 %
	2	90.7 %
	5	96.0 %
	10	98.0 %

from the use of closed-loop DBS compared to open-loop DBS during a 480 s are presented in Table III for the two simulated STN populations. Large reductions in energy were observed when the STN was weakly coupled to the remainder of the network, since the stimulus amplitude remained at zero for a large proportion of the stimulation period. As the gain of the controller was increased, the energy reduction for cases of weak coupling also increased. Strongly coupled networks, however, predicted a decrease in the energy reduction provided by closed-loop stimulation as controller gain was increased.

E. DBS response to transient increase in beta-band activity

The performance of the controller in the presence of a step change in the loop gain occurring at 200 s and a reset to the original loop gain at 300 s is presented in Figure 7, for a controller gain of 1. The increased gain promotes the re-growth of beta-band oscillations, shown by the increased magnitude of the beta-band LFP and biomarker signal, Figure 7. In both the strongly coupled and weakly coupled cases, the controller then increased the DBS amplitude to quench the increased beta-band oscillations, Figure 7(a) and Figure 7(b). The reduction in the energy delivered by using closed-loop stimulation in comparison to open-loop stimulation in the presence of temporarily increased gain was 35.3 % when the STN was strongly coupled to the remainder of the network and 54.3 % when the STN was weakly coupled to the remainder of the network.

IV. DISCUSSION

The aim of this study was to develop a new model to integrate volume conduction effects into a network model of pathological beta-band oscillations in order to investigate the feasibility of closed-loop high-frequency DBS through simulation. The hybrid architecture of the model developed in this study, using both physiologically-based and phenomenological mean-field representations of different nuclei in the basal ganglia, reduced the computational burden relative to entirely physiologically-based models, while enabling the effects of the volume conductor on neural activation and the simulated LFP to be incorporated. Based on reported experimental data, it was assumed that the strength of beta-band oscillations was directly related to the symptom severity, and on this basis the ARV of the beta-band LFP was used as the error signal for the closed-loop DBS controller. Clinical studies have reported a reduction in the level of beta-band activity following the application of DBS [8], [4], leading to the LFP's being suggested as a biomarker for use in the design of closed-loop DBS [9]. Whilst computational investigations of "mild" stimulation methods, such as coordinated reset and mean field feedback, suggest a return to physiological network activity [12], [13], [14], closed-loop high frequency DBS relies on the same underlying mechanisms of action as open-loop DBS. It is likely that closed-loop high frequency DBS would be more immediately suitable for implementation than alternative closed-loop methods, due to the similarity of the signal generation circuitry to current open-loop technology.

In the absence of DBS, under conditions of simulated dopamine depletion the network exhibited beta-band oscillations in each nucleus at approximately 22 Hz, with parkinsonian bursting characteristics evident in the STN, Figure 4(a). The power spectrum of the simulated LFP contained substantial power within the beta-band, as observed in electrophysiological studies [6], [47]. When open-loop DBS was applied, the simulated LFP and resulting biomarker decreased

in magnitude as the pathological oscillations were quenched. The application of closed-loop integral control of the DBS amplitude, based on the ARV of the LFP reduced the stimulation amplitude once the initial desynchronisation had occurred, Figure 6. Neurons whose threshold for axonal activation lay below the amplitude of the DBS signal fired in synchrony with the DBS signal, whilst remaining members of the population progressively ceased firing. Regardless of the network configuration examined, closed-loop stimulation consistently provided a saving in energy when compared to the open-loop stimulation paradigm, Table III. These savings suggest that closed-loop stimulation may reduce the frequency at which battery replacement surgeries are required, as the power consumption of the IPG is reduced. However, the amount of energy saved depended on the strength of coupling of the STN neurons to other nuclei in the network and on the controller gain used.

Energy reductions of up to 83.5 % were observed over the 480 s period examined for low controller gains when relatively weak coupling between the STN and GPe, and between the STN and cortex, was simulated, Table III. In this case, the stimulus amplitude was gradually reduced to zero once desynchronisation had occurred, Figure 6. In the weakly coupled case, synaptic noise within the oscillatory loop was insufficient, given the relatively low network gains, to re-establish oscillations. However, once STN firing has been elicited by a transient input, the network gain together with the nonlinear response of the STN was sufficient to regenerate and sustain the oscillation. The bistability in the weakly coupled case is broadly compatible with experimental results that show a prolonged attenutation of beta-band activity following the cessation of stimulation [6]. The results are also consistent with the coordinated reset mild stimulation paradigm, proposed by [11], suggesting that closed-loop high frequency DBS in a weakly coupled network may have similar functional behaviour. Energy reductions were of lower magnitude in cases where the STN was strongly coupled to the rest of the network, 39.1 % to 41.9 %, for a controller gain of 1. In the case of strong coupling, the oscillations re-established rapidly as the stimulation amplitude was reduced, requiring a continuous low-level stimulation to be maintained. In this case, synaptic noise inputs promoted subtheshold oscillations in the mean field that rapidly attained sufficient magnitude to elicit firing of the STN neurons.

The effect of increasing controller gain also depended on the coupling strength of the STN to the network, Table III. When the STN was strongly coupled to the network, increasing controller gain resulted in increased instability of the control output, resulting in the stimulation cycling on and off, thus reducing the energy savings achieved by the closed-loop controller as the integral gain was increased. In contrast, when the STN was weakly coupled, the energy reduction with increasing controller gain was higher since the DBS amplitude returned to zero earlier and remained off. Based on these observations, tuning of controller parameters to minimise the delivered stimulus energy will depend on the coupling strength of the target STN neurons to each other and to the remainder of the basal ganglia network.

The control scheme exhibited the ability to adapt to changing conditions without readjustment of the control parameters. For example, when increased levels of beta activity were promoted by an additional increase in the network gain, the controller responded by increasing the applied DBS amplitude, Figure 7. The ability to respond in a stable manner to simulated disturbances was observed regardless of the strength of the network coupling.

Integral control was chosen in preference to other schemes, such as proportional-integral control, principally because the number of axons activated with respect to the stimulation voltage is non-linear, causing the performance of a linear proportional control path to be unpredictable. In addition, integral control avoids the steady-state error associated with proportional control. Although proportional control may provide acceptable performance in the case of weakly-coupled networks, the inherent absence of of a steady-state error ensured that integral control functioned with both weakly and strongly connected networks. It is possible that alternative control architectures may provide higher energy savings and more effective symptom control than pure integral control. Adaptive control schemes that can alter the controller parameters in response to changes in the network could realize further reductions in stimulus energy in both strongly and weakly coupled networks.

The model used in this simulation study is by its nature a simplified representation of a highly complex system, and therefore contains a number of important limitations. In the examples presented, a subset of all possible oscillatory networks was simulated, and certain pathways have not been incorporated. These include direct projections from the thalamus to the STN [48], and the striatum itself, along with its projections to the GPe. DBS elicited its effects through direct axonal activation. This assumption neglected somatic inhibition effects that may be present, where the summation of dendritic currents induced by DBS hyperpolarizes the cell body [21]. Such effects could prevent the transmission of network oscillatory activity and further alter the required stimulation amplitude. In this study, axonal activation was defined as occuring when the axon responds to 100 % of simulus pulses, in contrast to a lower proportion as defined in previous studies [49]. Definition of activation as response to less than 100 % of stimulus pulses could further reduce the stimulation energy required under closed-loop DBS. The single-cell STN model described in [43] includes only a subset of ion channels present in the STN [44], [50], [51]. Additionally, it has been shown in other studies that DBS may alter the firing rates of STN neurons without bringing them into synchrony with the stimulation signal [22].

Modeling studies have suggested that DBS targeted at the STN may achieve a portion of its clinical benefit by activating fibers in other nuclei [18], an effect that is neglected in this model, but which may further reduce the required stimulation. The use of a mean-field network did not allow changes in firing patterns under parkinsonian conditions and during DBS in nuclei other than the STN to be individually observed, as only the presence or absence of synchronised oscillator behaviour was considered. Unsynchronised physiological firing in the

STN was therefore not simulated. Furthermore, the mean field signal was directly connected to the STN neurons, without modelling the exponential characteristic of the excitatory post-synaptic potential. Although the simulated LFP included stimulus artifact, its lowest harmonic was above the upper stop band of the bandpass filter in the controller, since the model assumed the electrodes to be ideal conductors with no interface layer. In reality, a non-ideal electrode-tissue interface may cause additional nonlinear distortion of the stimulus artifact that is within the passband of the filter at the control input. A number of artifact subtraction schemes have been previously proposed and could be incorporated in clinical implementations of closed-loop DBS to mitigate this limitation [52], [53], [54]. The LFP was simulated as a monopolar recording, however clinical studies tend to record the LFP in bipolar configurations, which may allow more focal recordings [3], [55]. This was unnecessary in the present study as the simulated LFP could be attributed entirely to the STN. The criterion used to set the parameters of the model was sufficient loop gain, simulating cumalative synaptic gain, to promote the establishment of beta-band oscillation without reference to the individual components of the cortical loop. For example, certain pathways have been shown to be strengthened and others weakened in conditions of dopamine depletion, [37], [40]. While this study considered monopolar voltage-controlled stimulation, the most common clinically used configuration [56], similar controller performance would be expected if bipolar or current-controlled stimulation were used. The results presented in [28] suggest that the choice of a resistive volume conductor model may cause an over or under-estimation of the axonal activation to occur in the two networks examined. Changes in tissue properties may also alter threshold stimulation amplitudes for axons and the amplitude of the LFP, however this would remain a numerical scaling since the volume conductor is assumed to be piecewise homogeneous. Further errors in the axonal activation common to all networks could be caused by non-idealities in the stimulation waveform, which have not been considered here [57]. Finally synaptic changes due to DBS have been hypothesized by closed-loop modeling studies [58], but were neglected in this study and may have implications for controller tuning if the effective coupling strength were to change.

V. Conclusion

A new model was developed in which volume conductor effects of DBS were incorporated into a model of the pathological beta-band oscillations in the basal ganglia. The model was used to simulate closed-loop control of the amplitude of high frequency DBS. The results provide support for the clinical hypothesis that it may be possible to apply closed-loop DBS based on the ARV of the beta-band LFP activity recorded from the STN using the DBS electrode. The reduction in stimulus energy estimated when open-loop DBS was replaced by closed-loop DBS depended on the strength of the coupling between the STN and the other nuclei, and on the gain of the controller. Integral closed-loop control was also found to be capable of adapting to changes in the level of beta activity. The simulation results support the use of closed-loop high-frequency DBS, in the short-term, based on electrophysiological biomarkers that can be implemented using existing technologies [15].

References

[1] K. Ashkan, B. Wallace, B. A. Bell, and A. L. Benabid, "Deep brain stimulation of the subthalamic nucleus in parkinson's disease 1993-2003: where are we 10 years on?" *Br J Neurosurg*, vol. 18, no. 1, pp. 19–34, 2004.

[2] P. Brown and D. Williams, "Basal ganglia local field potential activity: character and functional significance in the human," *Clin Neurophysiol*, vol. 116, no. 11, pp. 2510–9, Nov 2005.

[3] A. G. Androulidakis, C. Brücke, F. Kempf, A. Kupsch, T. Aziz, K. Ashkan, A. A. Kühn, and P. Brown, "Amplitude modulation of oscillatory activity in the subthalamic nucleus during movement," *Eur J Neurosci*, vol. 27, no. 5, pp. 1277–84, Mar 2008.

[4] A. A. Kühn, F. Kempf, C. Brücke, L. Gaynor Doyle, I. Martinez-Torres, A. Pogosyan, T. Trottenberg, A. Kupsch, G.-H. Schneider, M. I. Hariz, W. Vandenberghe, B. Nuttin, and P. Brown, "High-frequency stimulation of the subthalamic nucleus suppresses oscillatory beta activity in patients with parkinson's disease in parallel with improvement in motor performance," *J Neurosci*, vol. 28, no. 24, pp. 6165–73, Jun 2008.

[5] P. Brown and A. Eusebio, "Paradoxes of functional neurosurgery: clues from basal ganglia recordings," *Mov Disord*, vol. 23, no. 1, pp. 12–20; quiz 158, Jan 2008.

[6] H. Bronte-Stewart, C. Barberini, M. M. Koop, B. C. Hill, J. M. Henderson, and B. Wingeier, "The STN beta-band profile in parkinson's disease is stationary and shows prolonged attenuation after deep brain stimulation," *Exp Neurol*, vol. 215, no. 1, pp. 20–8, Jan 2009.

[7] C. de Solages, B. C. Hill, M. M. Koop, J. M. Henderson, and H. Bronte-Stewart, "Bilateral symmetry and coherence of subthalamic nuclei beta band activity in parkinson's disease," *Exp Neurol*, vol. 221, no. 1, pp. 260–6, Jan 2010.

[8] B. Wingeier, T. Tcheng, M. M. Koop, B. C. Hill, G. Heit, and H. M. Bronte-Stewart, "Intra-operative STN DBS attenuates the prominent beta rhythm in the STN in parkinson's disease," *Exp Neurol*, vol. 197, no. 1, pp. 244–51, Jan 2006.

[9] A. Eusebio and P. Brown, "Synchronisation in the beta frequency-band–the bad boy of parkinsonism or an innocent bystander?" *Exp Neurol*, vol. 217, no. 1, pp. 1–3, May 2009.

[10] S. Santaniello, G. Fiengo, L. Glielmo, and W. M. Grill, "Closed-loop control of deep brain stimulation: a simulation study," *IEEE Trans Neural Syst Rehabil Eng*, vol. 19, no. 1, pp. 15–24, Feb 2011.

[11] C. Hauptmann and P. A. Tass, "Cumulative and after-effects of short and weak coordinated reset stimulation: a modeling study," *J Neural Eng*, vol. 6, no. 1, p. 016004, Feb 2009.

[12] M. Rosenblum and A. Pikovsky, "Delayed feedback control of collective synchrony: an approach to suppression of pathological brain rhythms," *Phys Rev E Stat Nonlin Soft Matter Phys*, vol. 70, no. 4 Pt 1, p. 041904, Oct 2004.

[13] O. V. Popovych, C. Hauptmann, and P. A. Tass, "Impact of nonlinear delayed feedback on synchronized oscillators," *J Biol Phys*, vol. 34, no. 3-4, pp. 267–79, Aug 2008.

[14] Y. Guo and J. E. Rubin, "Multi-site stimulation of subthalamic nucleus diminishes thalamocortical relay errors in a biophysical network model," *Neural Netw*, vol. 24, no. 6, pp. 602–16, Aug 2011.

[15] S. Jensen, G. Molnar, J. Giftakis, W. Santa, R. Jensen, D. Carlson, M. Lent, and T. Denison, "Information, energy, and entropy: Design principles for adaptive, therapeutic modulation of neural circuits," in *34th European Solid-State Circuits Conference*, 2008.

[16] X.-J. Feng, E. Shea-Brown, B. Greenwald, R. Kosut, and H. Rabitz, "Optimal deep brain stimulation of the subthalamic nucleus–a computational study." *J Comput Neurosci*, vol. 23, no. 3, pp. 265–282, 2007.

[17] X.-J. Feng, B. Greenwald, H. Rabitz, E. Shea-Brown, and R. Kosut, "Toward closed-loop optimization of deep brain stimulation for parkinson's disease: concepts and lessons from a computational model." *J Neural Eng*, vol. 4, no. 2, pp. L14–21, 2007.

[18] S. N. Sotiropoulos and P. N. Steinmetz, "Assessing the direct effects of deep brain stimulation using embedded axon models." *J Neural Eng*, vol. 4, no. 2, pp. 107–119, 2007.

[19] P. J. Hahn and C. C. McIntyre, "Modeling shifts in the rate and pattern of subthalamopallidal network activity during deep brain stimulation," *J Comput Neurosci*, Mar 2010.

[20] A. M. de Paor and M. M. Lowery, "Analysis of the mechanism of action of deep brain stimulation using the concepts of dither injection and the equivalent nonlinearity," *IEEE Trans Biomed Eng*, vol. 56, no. 11 Pt 2, pp. 2717–20, Nov 2009.

[21] C. C. McIntyre, W. M. Grill, D. L. Sherman, and N. V. Thakor, "Cellular effects of deep brain stimulation: model-based analysis of activation and inhibition." *J Neurophysiol*, vol. 91, no. 4, pp. 1457–1469, 2004.

[22] N. Yousif, N. Purswani, R. Bayford, D. Nandi, P. Bain, and X. Liu, "Evaluating the impact of the deep brain stimulation induced electric field on subthalamic neurons: A computational modelling study," *J Neurosci Methods*, Jan 2010.

[23] P. F. Grant and M. M. Lowery, "Electric field distribution in a finite-volume head model of deep brain stimulation," *Med Eng Phys*, vol. 31, no. 9, pp. 1095–103, Nov 2009.

[24] G. Walckiers, B. Fuchs, J.-P. Thiran, J. R. Mosig, and C. Pollo, "Influence of the implanted pulse generator as reference electrode in finite element model of monopolar deep brain stimulation," *J Neurosci Methods*, vol. 186, no. 1, pp. 90–6, Jan 2010.

[25] Medtronic, Inc., *3387-3389 Lead Kit for Deep Brain Stimulation - Implant Manual*, Minneapolis, MA, 2006.

[26] A. M. R. Agur, J. M. Lee, and J. C. B. Grant, *Grant's Atlas of Anatomy*. Lippincott, Williams and Wilkins, 1999.

[27] W. M. Grill and J. T. Mortimer, "Electrical properties of implant encapsulation tissue." *Ann Biomed Eng*, vol. 22, no. 1, pp. 23–33, Sep 1994.

[28] P. F. Grant and M. M. Lowery, "Effect of dispersive conductivity and permittivity in volume conductor models of deep brain stimulation," *IEEE Trans Biomed Eng*, vol. 57, no. 10, pp. 2386–2393, Oct 2010.

[29] O. Scheufler, N. M. Kania, C. M. Heinrichs, and K. Exner, "Hyperplasia of the subcutaneous adipose tissue is the primary histopathologic abnormality in lipedematous scalp." *Am J Dermatopathol*, vol. 25, no. 3, pp. 248–252, 2003.

[30] International commission of radiological protection, *Report of the Task Group on Reference Man*. Oxford Pergamon Press, 1975.

[31] C. R. Butson, C. B. Maks, and C. C. McIntyre, "Sources and effects of electrode impedance during deep brain stimulation." *Clin Neurophysiol*, vol. 117, no. 2, pp. 447–454, 2006.

[32] S. Gabriel, R. W. Lau, and C. Gabriel, "The dielectric properties of biological tissues: III. parametric models for the dielectric spectrum of tissues." *Phys Med Biol*, vol. 41, no. 11, pp. 2271–2293, 1996.

[33] S. B. Baumann, D. R. Wozny, S. K. Kelly, and F. M. Meno, "The electrical conductivity of human cerebrospinal fluid at body temperature." *IEEE Trans Biomed Eng*, vol. 44, no. 3, pp. 220–223, 1997.

[34] J. B. J. Ranck and S. L. BeMent, "The specific impedance of the dorsal columns of the cat: an inisotropic medium." *Exp Neurol*, vol. 11, pp. 451–463, 1965.

[35] C. C. McIntyre, A. G. Richardson, and W. M. Grill, "Modeling the excitability of mammalian nerve fibers: influence of afterpotentials on the recovery cycle." *J Neurophysiol*, vol. 87, no. 2, pp. 995–1006, Feb 2002.

[36] R. Levy, W. D. Hutchison, A. M. Lozano, and J. O. Dostrovsky, "High-frequency synchronization of neuronal activity in the subthalamic nucleus of parkinsonian patients with limb tremor," *J Neurosci*, vol. 20, no. 20, pp. 7766–75, Oct 2000.

[37] A. Leblois, T. Boraud, W. Meissner, H. Bergman, and D. Hansel, "Competition between feedback loops underlies normal and pathological dynamics in the basal ganglia," *J Neurosci*, vol. 26, no. 13, pp. 3567–83, Mar 2006.

[38] A. V. Cruz, N. Mallet, P. J. Magill, P. Brown, and B. B. Averbeck, "Effects of dopamine depletion on network entropy in the external globus pallidus," *J Neurophysiol*, vol. 102, no. 2, pp. 1092–102, Aug 2009.

[39] N. Mallet, A. Pogosyan, L. F. Márton, J. P. Bolam, P. Brown, and P. J. Magill, "Parkinsonian beta oscillations in the external globus pallidus and their relationship with subthalamic nucleus activity," *J Neurosci*, vol. 28, no. 52, pp. 14 245–58, Dec 2008.

[40] R. J. Moran, N. Mallet, V. Litvak, R. J. Dolan, P. J. Magill, K. J. Friston, and P. Brown, "Alterations in brain connectivity underlying beta oscillations in parkinsonism," *PLoS Comput Biol*, vol. 7, no. 8, p. e1002124, Aug 2011.

[41] Y. Kuramoto, *Chemical Oscillations, Waves and Turbulence*. Springer-Verlag, 1984.

[42] A. Nambu, "A new approach to understand the pathophysiology of parkinson's disease," *J Neurol*, vol. 252 Suppl 4, pp. IV1–IV4, Oct 2005.

[43] T. Otsuka, T. Abe, T. Tsukagawa, and W.-J. Song, "Conductance-based model of the voltage-dependent generation of a plateau potential in subthalamic neurons," *J Neurophysiol*, vol. 92, no. 1, pp. 255–64, Jul 2004.

[44] C. Beurrier, P. Congar, B. Bioulac, and C. Hammond, "Subthalamic nucleus neurons switch from single-spike activity to burst-firing mode," *J Neurosci*, vol. 19, no. 2, pp. 599–609, Jan 1999.

[45] H. M. Power and R. J. Simpson, *Introduction to Dynamics and Control*. McGraw Hill, 1978.

[46] M. L. Hines and N. T. Carnevale, "Neuron: a tool for neuroscientists," *Neuroscientist*, vol. 7, no. 2, pp. 123–35, Apr 2001.

[47] M. Weinberger, N. Mahant, W. D. Hutchison, A. M. Lozano, E. Moro, M. Hodaie, A. E. Lang, and J. O. Dostrovsky, "Beta oscillatory activity in the subthalamic nucleus and its relation to dopaminergic response in parkinson's disease," *J Neurophysiol*, vol. 96, no. 6, pp. 3248–56, Dec 2006.

[48] A. Gillies and D. Willshaw, "Models of the subthalamic nucleus. the importance of intranuclear connectivity," *Med Eng Phys*, vol. 26, no. 9, pp. 723–32, Nov 2004.

[49] S. Miocinovic, M. Parent, C. R. Butson, P. J. Hahn, G. S. Russo, J. L. Vitek, and C. C. McIntyre, "Computational analysis of subthalamic nucleus and lenticular fasciculus activation during therapeutic deep brain stimulation." *J Neurophysiol*, vol. 96, no. 3, pp. 1569–1580, 2006.

[50] Z.-T. Zhu, A. Munhall, K.-Z. Shen, and S. W. Johnson, "Calcium-dependent subthreshold oscillations determine bursting activity induced by n-methyl-d-aspartate in rat subthalamic neurons in vitro," *Eur J Neurosci*, vol. 19, no. 5, pp. 1296–304, Mar 2004.

[51] J. F. Atherton, K. Kitano, J. Baufreton, K. Fan, D. Wokosin, T. Tkatch, R. Shigemoto, D. J. Surmeier, and M. D. Bevan, "Selective participation of somatodendritic hcn channels in inhibitory but not excitatory synaptic integration in neurons of the subthalamic nucleus," *J Neurosci*, vol. 30, no. 47, pp. 16 025–40, Nov 2010.

[52] T. Hashimoto, C. M. Elder, and J. L. Vitek, "A template subtraction method for stimulus artifact removal in high-frequency deep brain stimulation," *J Neurosci Methods*, vol. 113, no. 2, pp. 181–6, Jan 2002.

[53] C. Waddell, J. Pratt, B. Porr, and S. Ewing, "Deep brain stimulation artifact removal through under-sampling and cubic-spline interpolation," in *2nd International Congress on Image and Signal Processing*, oct. 2009, pp. 1 –5.

[54] K. W. McCairn and R. S. Turner, "Deep brain stimulation of the globus pallidus internus in the parkinsonian primate: local entrainment and suppression of low-frequency oscillations," *J Neurophysiol*, vol. 101, no. 4, pp. 1941–60, Apr 2009.

[55] A. A. Kuhn, A. Tsui, T. Aziz, N. Ray, C. Brucke, A. Kupsch, G.-H. Schneider, and P. Brown, "Pathological synchronisation in the subthalamic nucleus of patients with parkinson's disease relates to both bradykinesia and rigidity." *Exp Neurol*, vol. 215, no. 2, pp. 380–387, Feb 2009.

[56] J. Volkmann, J. Herzog, F. Kopper, and G. Deuschl, "Introduction to the programming of deep brain stimulators." *Mov Disord*, vol. 17 Suppl 3, pp. S181–7, 2002.

[57] C. R. Butson and C. C. McIntyre, "Differences among implanted pulse generator waveforms cause variations in the neural response to deep brain stimulation." *Clin Neurophysiol*, vol. 118, no. 8, pp. 1889–1894, 2007.

[58] C. Hauptmann and P. A. Tass, "Therapeutic rewiring by means of desynchronizing brain stimulation." *Biosystems*, vol. 89, no. 1-3, pp. 173–181, 2007.